

# Behavior of water in contact with model hydrophobic cavities and tunnels and carbon nanotubes

E.P. Schulz, L.M. Alarcón, and G.A. Appignanesi<sup>a</sup>

Sección Físicoquímica, INQUISUR-UNS-CONICET and Departamento de Química, Universidad Nacional del Sur, Avenida Alem 1253, 8000-Bahía Blanca, Argentina

Received 31 March 2011

Published online: 24 October 2011 – © EDP Sciences / Società Italiana di Fisica / Springer-Verlag 2011

**Abstract.** By means of molecular dynamics simulations we analyze the behavior of water in contact with model hydrophobic cavities and tunnels. We study the hydration and filling propensity of cavities and tunnels carved in alkane monolayers and, for comparison, we also study single-walled carbon nanotubes of similar size. Our results will determine the dependence of the filling propensity as a function of cavity size while revealing the dynamical nature of the process with alternation of filled and dry states. Concerning the tunnels built across the monolayer, we shall show that the minimum diameter in order to get filled is about twice as large as that for the carbon nanotubes, thus evidencing a more hydrophobic behavior. The existence of water-water hydrogen bonds, a necessary condition for penetration, will also be made evident.

## 1 Introduction

A deep comprehension of the behavior of interfacial and (nano) confined water is mandatory in central fields of research like solvation, reaction dynamics and biology [1–11]. In particular, the hydration properties of protein binding sites have been suggested to play a major role in the binding of ligands or in protein-protein association [9, 11]. From one side, ligands are expected to displace hydration water molecules from their protein binding site [9]. On the other hand, geometrically induced surface dehydration (by means of water inaccessible cavities) has been shown to be central for the existence of reactive sites responsible for protein binding [11]. In addition, the behavior of water confined in cylindrical pores or tunnels is also important both from the basic and the applied viewpoints. For instance, this behavior is relevant for water flow in aquaporins and proton flow in proton pumps and enzymes [8]. While it is generally believed that small protein cavities are empty [9], there is no general consensus on whether large protein cavities are filled or empty and certain experimental results on the subject are contradictory (even when certain large cavities seem to indeed present small clusters of confined water molecules) [8, 9]. In turn, it has been shown that subnanometric nonpolar cavities (spherical pores) remain empty, whereas water penetrates nanometric size ones [8, 12]. For example, the interiors of the spherical  $C_{180}$  and  $C_{140}$  fullerenes (the size of the last one being barely larger than 10 Å) have been shown to

present stability for filled states with small clusters of water molecules connected by strong hydrogen bonds [8, 12]. Additionally, the filling and the conduction of water in carbon nanotubes has been extensively studied [8, 13–15] and many different water phases have been discovered (from 1D trains of hydrogen-bonded water molecules at low nanotube radius to complex layered structures within larger nanotubes [8, 13–15]). It has also been shown that the hydrophobicity of the material is important since a small reduction of the van der Waals attraction between water and the carbon atoms induces the drying of previously filled nanotubes [8].

From the results gathered within the above-exposed context, a general trend observed in nonpolar cavity filling is the formation of clusters of water molecules bound by well-shaped hydrogen bonds (HB) [8]. This stability requirement is not surprising since such HB are expected to be very strong given the desolvation environment in which they are formed (with an “effective” dielectric constant much reduced as compared to that of bulk water) [11, 16]. This strengthening of Coulombic interactions in desolvation environments has been recognized in biophysics [11, 16] and has been regarded as central for the protein binding process [11, 16]. This is so since soluble proteins tend to wrap or bury their intramolecular interactions (HB and salt bridges) in order to be stable in water (this protection is performed by surrounding the intramolecular interaction with hydrophobic residues which induce water removal). In turn, underwrapped intramolecular protein interactions (or dehydrons [11, 16]) are unshielded from water attack. Thus, such motifs are sticky

<sup>a</sup> e-mail: appignan@criba.edu.ar

since they promote further removal of surrounding water (which otherwise would disrupt the intramolecular interaction) and have thus been shown to be central for the protein-protein association phenomena upon which most biological functions rely [11, 16]. This paradox of reconciling stability with reactivity (which implies to reformulate the previous question of “how to keep dry in water?” [17] towards “how to do it without sacrificing reactivity?”) has been shown to be resolved by the role of geometry [11]. Underwrapped reactive sites on the surface protein have been shown by our group to be exclusively arranged in subnanometric cavities which thus provide a geometric shield to water attack (a level of local ruggedness completely absent at well-wrapped sites). This geometrical protection exploits the other related above-expounded trend in non-polar cavity filling: that water molecules do not penetrate in cavities of subnanometric sizes [8, 11]. This fact has been explained to be due to the reluctance of the water molecules to resign HB coordination with other water molecules (only nanometric size cavities allow the water molecules to penetrate retaining the HB coordination typical at surfaces) [11].

Within this context, the aim of the present work is to explore, by means of molecular dynamics simulations, the behavior of water in contact with model hydrophobic cavities and their filling tendencies. We use simple model hydrophobic surfaces in order to retain only the geometrical constraints which are nonetheless expected to play a central role (thus avoiding the more complicated chemical specificity and heterogeneity present in more realistic systems like proteins). First, we shall study the hydration of cavities carved in alkane monolayers. These cavities are expected to be more hydrophobic than other nonpolar pores studied in the past (like the interior of fullerenes) and thus the geometric constraints are expected to completely dominate the filling/drying propensities. In turn, we shall analyze the filling of tunnels generated in such monolayers and, for comparison, we shall also study single-walled carbon nanotubes of similar radii. Our results will determine the filling behavior as a function of cavity size and will also reveal the dynamical nature of the process with alternation of filled and dry states. As regards the tunnels, we shall show that the ones built across the monolayer require a larger radius in order to get filled as compared to the carbon nanotubes. The role of hydrogen bonding for cavity filling will also be made evident.

## 2 Methodology

### 2.1 Model systems

For the hydrophobic cavities we constructed a monolayer of 81 chains ( $9 \times 9$ ) of n-heptadecane ( $\text{CH}_3-(\text{CH}_2)_{15}-\text{CH}_3$ ) aligned in a parallel fashion so as to generate a cube. This arrangement mimics the monolayer structure of stearic acid chains adopted at a water interface but replaces the acid group (COOH) by a H so that the chain ends with a

metile, *i.e.* it becomes an n-heptadecane chain. The original chain separation was  $4.53 \text{ \AA}$ , the typical distance in a fatty acid monolayer. The monolayer was solvated with water molecules modeled by the TIP3P model [18, 19] with a canonical NVE ensemble with a Berendsen thermostat [20]. All simulations were done using the AMBER10 molecular simulation suite [21] with a 2 fs time step (we used the GAFF and FF99SB force fields). All calculations were performed in the NPT ensemble with a Langevin thermostat at  $T = 300 \text{ K}$ . The monolayer was solvated with TIP3P water molecules in an orthogonal cubic box with periodic boundary conditions. The size of the box was such that it extended more than  $20 \text{ \AA}$  away from all the monolayer faces. The surface monolayer was centered in the middle of the box. This monolayer without a hole will be called “perfect” monolayer from now on. For the cavities, we carved holes in the monolayer surface parallel to the  $(x, y)$ -plane in the  $z$ -direction (the position of the hydrogens at the top of the monolayer was  $z = 42.5 \text{ \AA}$  while the corresponding carbon atoms were placed at  $z = 41.6 \text{ \AA}$ . In all cases (perfect monolayer or with the different carved holes) the AMBER equilibration reduced the distance between the n-heptadecane molecules (the chain separation) to  $4.2 \text{ \AA}$ . To generate the cavities we carved squared holes of different sizes at the center of the monolayer surface by cutting the corresponding number of chains (the bonds of the carbon atoms at the bottom of the hole were saturated so that all chains ended with a methyl group; in other words, they became shorter chain alkanes). For the holes we shall use the following nomenclature:  $A \times B$  means that the chains of a number  $A$  of molecules conforming a square at the center of the monolayer were shortened in  $B$  units (the depth of the hole is thus given by  $B \times 1.2 \text{ \AA}$  where  $1.2 \text{ \AA}$  is the length of a  $\text{CH}_2$  monomer). The numerical relation between  $A$  and  $B$  was such that approximately the “radius” of the hole (as we shall call from now on the measure that corresponds to half the length of the square conforming the “mouth” of the hole) was as close as possible to the hole depth. For illustration, in fig. 1 (top) we show a configuration of the monolayer with a  $9 \times 7$  hole solvated with water molecules. We studied  $1 \times 3$ ,  $4 \times 5$ ,  $9 \times 7$ ,  $16 \times 9$ , and  $25 \times 11$  holes, together with the perfect monolayer. The larger holes were carved on larger size monolayers so that in all simulations, we always have holes which are far enough from the borders of the  $(x, y)$  surface of the monolayer. For the tunnels we used a similar nomenclature and thus, tunnel 1, tunnel 4 and tunnel 9 refer to the situation where we extracted respectively 1, 4 and 9 complete chains at the center of the monolayer, so that both the upper and lower faces of the monolayer cube were connected by the tunnel. In fig. 1 (bottom) we show an example of a tunnel (tunnel 4). In turn, the single-walled carbon nanotubes employed had radii 2.0, 3.9, 4.75, 8.15, 12.25, 20.4 and  $67.5 \text{ \AA}$ . Each of the nanotubes was solvated in a box of TIP3P water molecules that extended more than  $20 \text{ \AA}$  away from the nanotube borders in each direction. The axis of the nanotube coincided with the  $x$ -axis and the length of the nanotubes was  $14 \text{ \AA}$  in all cases.

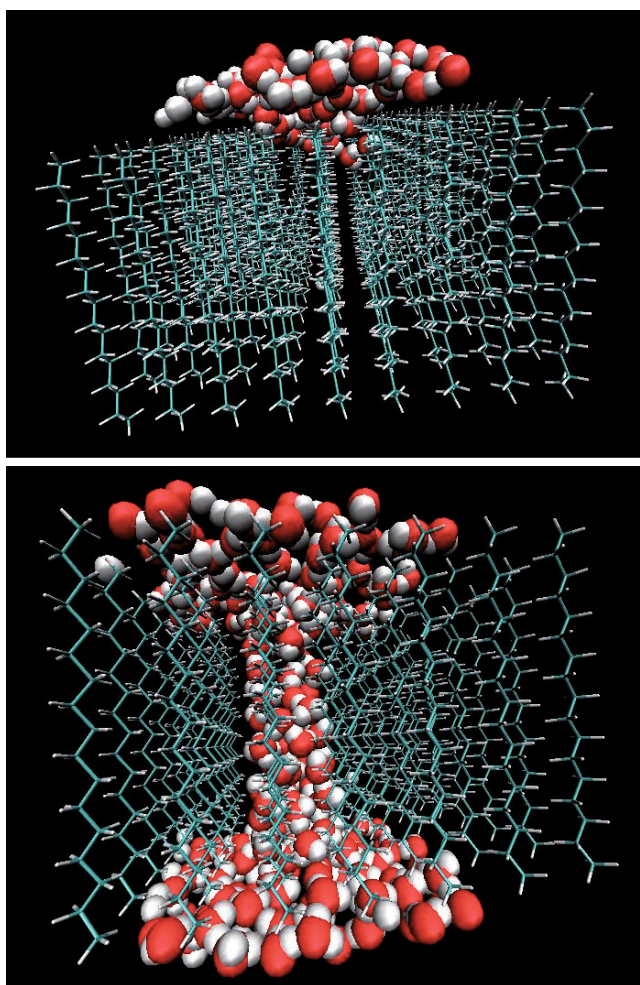


**Fig. 1.** Top: snapshot of the simulation of a  $9 \times 7$  hole monolayer. Bottom: idem for tunnel 4. In order to better illustrate the hole and the tunnel, in both cases we have only included a few of the water molecules. We recall that all the six faces of the monolayers are completely surrounded by  $20 \text{ \AA}$  of water molecules.

## 3 Results

### 3.1 Hydrophobic cavities

Figure 2 shows the density profile along the  $z$ -direction, the normal to the monolayer surface (which lies in the  $(x, y)$ -plane). We can see that the perfect monolayer displays the typical behavior found for other nonpolar surfaces [10]. The small  $1 \times 3$  hole is empty and the hydration water layer does not seem to “feel” the presence of the hole since it adopts an almost planar arrangement parallel to the surface. For larger cavity sizes the hydration water layer begins to “notice” the presence of the hole and the plane of vicinal water molecules begins to present a deformation at the position of the hole (begins to get closer to the monolayer at the hole position). At even larger holes the water molecules clearly penetrate into the cavity.

In order to better determine whether water is able to fill the different cavities, we calculated the minimum  $z$

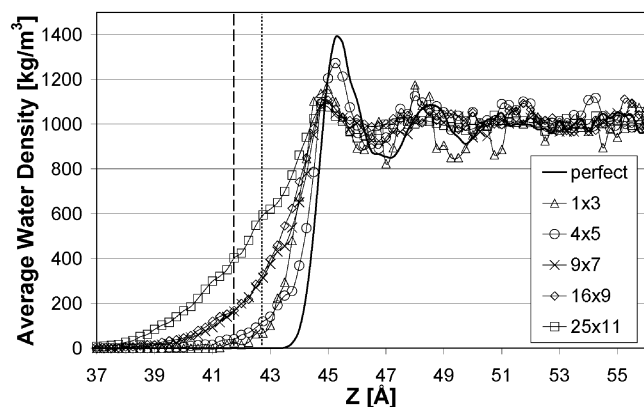


**Fig. 2.** Density profile for the water molecules in the direction normal to the surface of the perfect monolayer and for the ones with cavities  $1 \times 3$ ,  $4 \times 5$ ,  $9 \times 7$ ,  $16 \times 9$  and  $25 \times 11$ . In such graph we indicate the positions of the C (dashed line) and the H (dotted line) atoms at the surface of the monolayer. These marks can be taken as the border of the cavity which extends in the decreasing  $z$ -direction.

value (maximum penetration) reached by any of the water molecules as a function of time. These results are shown in fig. 3 where we can see that filling is not homogeneous in time. Instead, this plot makes evident the fact that filling and drying represent dynamical processes. The small  $1 \times 3$  hole is empty almost all the time since the profile is very similar to that for the perfect monolayer (only very seldom the water molecules penetrate the depth of the line indicating the border of the hole, which we estimate here as the  $z$  position of the topmost H atoms of the perfect monolayer). For larger intermediate-size cavities, however, we can see that the system alternates between periods when the water molecules penetrate or fill the cavity (water molecules below the  $z$  position of the border of the cavity) and dry periods. At the times when the hole is empty the water molecules are located roughly at the same  $z$  position as the water molecules hydrating the perfect monolayer. Thus, these cavities show an alternation of empty and filled states with the fraction of time filled increasing as the cavity size increases. This is an interesting result since the water molecules tend to be either filling the cavity or else excluded from it as if there were no hole, without significant population of intermediate positions. Only the largest cavities (for example, the hole  $25 \times 11$  which has a diameter of  $25.3$  or  $21.7 \text{ \AA}$  when measured by the C-C chain distance or by its van der Waals diameter, respectively) are found to be filled almost all the simulation time. In fig. 4 we thus show the fraction of time filled,  $\phi$ , as a function of the cavity diameter (both measured from center to center of the chains, that is from C atom to C atom, and by its van der Waals diameter).

Another point worth mentioning is the effect of the abrupt nature of the sides (walls) of the holes on water penetration. To study this point we generated two other holes with less steep walls. We considered the  $9 \times 7$  and the  $25 \times 11$  holes sculpted in the following way: For the sculpted  $9 \times 7$  hole the central alkane chain was shortened

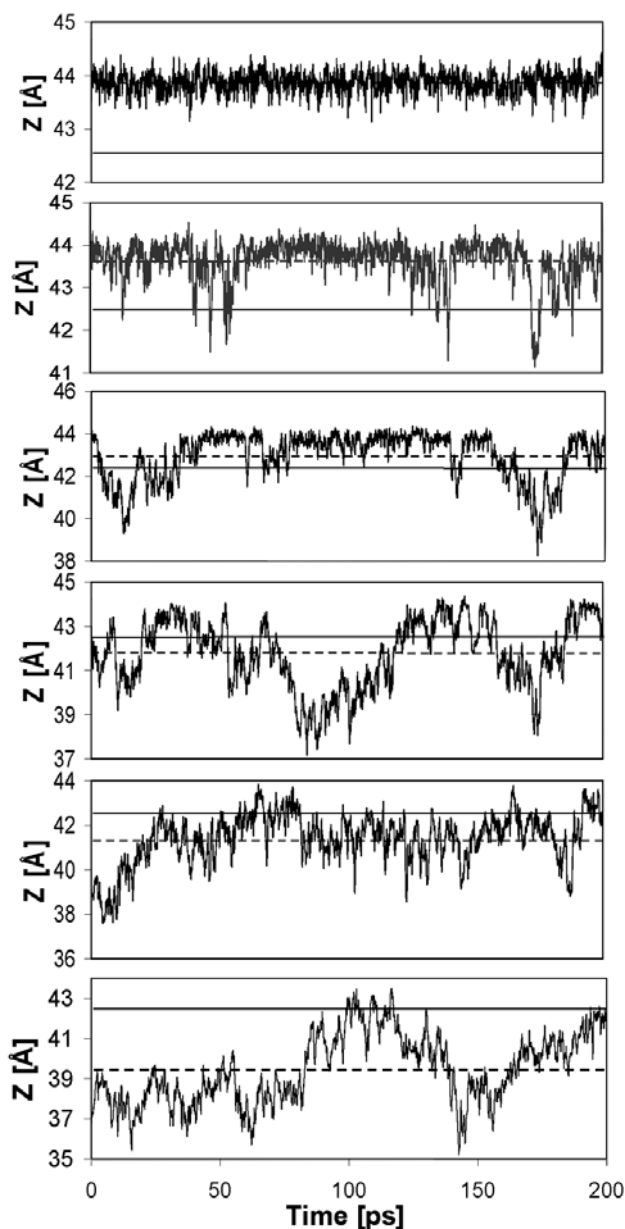


**Fig. 3.** Maximum penetration reached by the water molecules as a function of time for the different cavities (from top to bottom: perfect monolayer —*i.e.* without hole— and  $1 \times 3$ ,  $4 \times 5$ ,  $9 \times 7$ ,  $16 \times 9$ , and  $25 \times 11$  holes). In all cases, the solid horizontal lines indicate the position of the topmost H atoms of the monolayer and the dashed lines represent the time-averaged maximum water penetration.

in 7  $\text{CH}_2$  monomers (as was the case for the  $9 \times 7$  hole), its four first neighboring alkane chains were shortened in 5 monomers while the remaining four chains were shortened in 4 units. In turn, for the  $25 \times 11$  sculpted hole the central chain was shortened in 11 monomers (as for the  $25 \times 11$  hole), the surrounding 8 chains were shortened in 9 units and the remaining 16 chains of the outer square were shortened in 7 units. In fig. 5 we show the maximum water penetration as a function of time for both sculpted

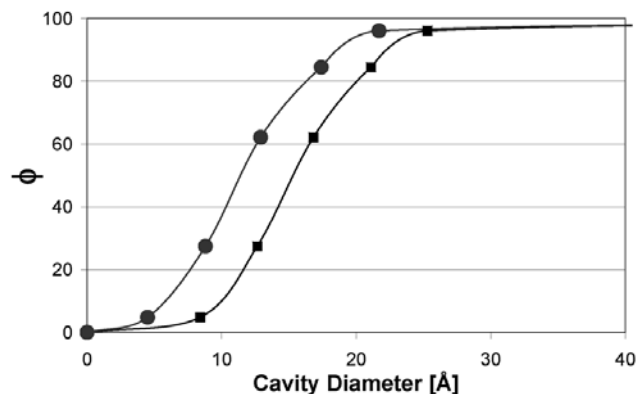


**Fig. 4.** Fraction of time filled,  $\phi$ , for the different cavities plotted as a function of cavity size. The squares correspond to the case when the cavity diameter is measured by the C-C chain separation while the circles indicate the case when the van der Waals radii of the atoms are taken into account. Lines are provided simply as a guide to the eye.

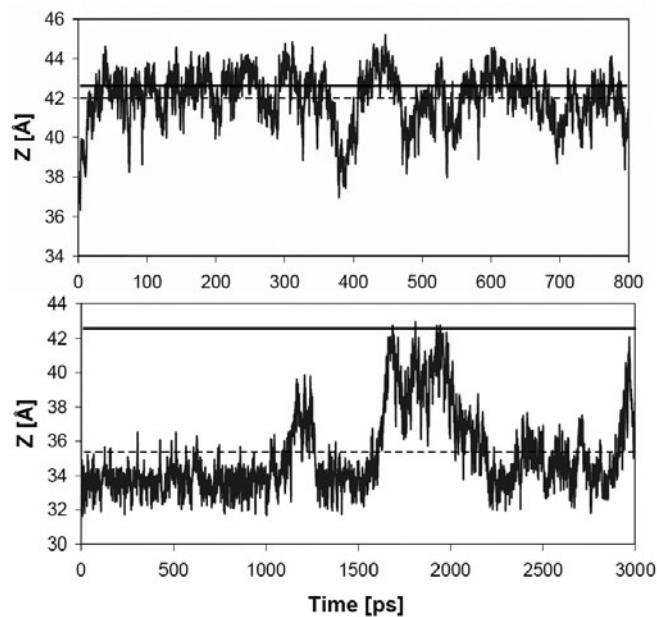


**Fig. 5.** Maximum penetration reached by the water molecules as a function of time for the two sculpted cavities (the figure at the top corresponds to the  $9 \times 7$  sculpted hole and the one at the bottom is for the  $25 \times 11$  sculpted hole). Again, the solid horizontal lines indicate the position of the topmost H atoms of the monolayer and the dashed lines represent the time-averaged maximum water penetration.

holes. We can see that the behavior of the sculpted  $9 \times 7$  hole is very similar to that of the former  $9 \times 7$  hole both regarding the fraction of time filled and the average water penetration. For the  $25 \times 11$  hole we can see that the fraction of time filled is similar to that of the former  $25 \times 11$  hole. However, in this case the average water penetration is greater and the water molecules are able to hydrate the

bottom of the hole: they reach a distance to the bottom similar to that of the hydration water molecules at the surface of the perfect monolayer. Thus, we can learn that the water-wall interactions are relatively important since they can increase the depth of cavity penetration while not altering significantly the time the cavity is filled.

### 3.2 Filling of hydrophobic tunnels and carbon nanotubes

When we solvated and equilibrated the three tunnels (tunnel 1, tunnel 4 and tunnel 9), we found that water was able to fill only tunnel 9: this tunnel remains filled with water molecules all the simulation time while the other ones remain empty. The size of tunnel 9 is 16.82 Å when measured by the C-C distance and 12.9 Å when its van der Waals diameter is considered. Thus, in order to get a better estimation of the minimum tunnel size that can be filled, we built new versions of tunnel 4 but from monolayers with greater chain separation (we recall that for the original tunnel 4 the chain separation after equilibration was 4.2 Å). When the chain separation after equilibration was 4.35 Å (thus implying a tunnel size of 13 Å or 9.3 Å when measured by the C-C distance or the van der Waals diameter, respectively) the tunnel remained empty and could only be filled when the chain separation reached 4.5 Å (tunnel size of 13.5 Å for C-C and 9.8 Å in van der Waals). This minimum tunnel size for filling is very large if compared to carbon nanotubes, since smaller diameter nanotubes have been found to be filled [8, 13–15]. For example, a train of hydrogen-bonded water molecules (a one-dimensional pattern) has been shown to penetrate a nanotube of 8.1 Å diameter measured by its C-C distance. This water arrangement did not form in our hydrophobic tunnels of comparable size. This fact might imply that the water-wall interactions stabilize such inner water structure. In turn, when water filled our larger tunnels, three-dimensional water arrangements occurred.

In order to compare our tunnels with carbon nanotubes in more detail, we constructed many carbon nanotubes of different diameters (from 4 to 100 Å diameter in C-C distance) and found that all nanotubes with a diameter larger than 7.0 Å/4.2 Å (in C-C or van der Waals diameters, respectively) were filled, while nanotubes with diameters lower than 6.2 Å/3.9 Å remained empty. Thus, the minimum size nanotube that can be filled by water is roughly half the diameter of the minimum tunnel size. This shows the importance of the water-wall interactions and implies that the tunnels are behaving in a more hydrophobic fashion as compared to the carbon nanotubes. This is also consistent with the result mentioned of nanotube dewetting when the water-wall interaction strength is decreased in simulations [8].

Finally, we mention that inside the tunnels we also found a great tendency for the water molecules to be engaged in hydrogen-bonded structures. Figure 6 shows a typical snapshot for the water molecules inside a tunnel.

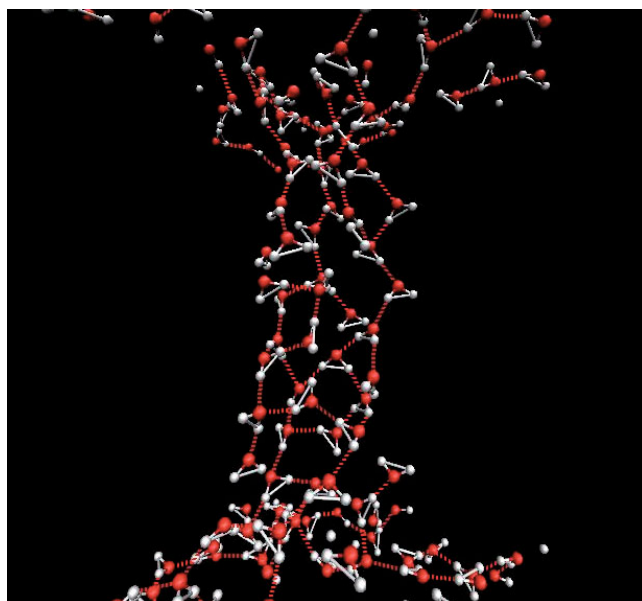


**Fig. 6.** A snapshot of the water molecules inside tunnel 4 displaying a typical arrangement. The width of this tunnel is 13.5 Å/9.8 Å (in C-C or van der Waals diameters, respectively). HBs are indicated by dotted lines. For the sake of clarity, we do not show the monolayer chains but only the inner water molecules and only a few other water molecules outside the tunnel.

The dotted lines indicate HBs calculated with a geometric criterion ( $O \cdots O$  distance lower than 3.2 Å and angle  $O-H \cdots O$  lower than 30°). We can easily observe many HBs between the inner molecules, even when ordered patterns are not easy to form given the high (ambient) temperature of the system.

## 4 Conclusions

In this work we have studied the behavior of water confined in model alkane-like hydrophobic cavities and tunnels and within carbon nanotubes. While subnanometric diameter cavities are empty most of the time, the filling of small nanometric cavities has been shown not to be homogeneous in time but to represent a dynamic process with alternation of filled and completely dry states. The larger cavities, in turn, tend to remain filled practically for all the simulation time. Additionally, we have found that the tunnels remain empty until about twice the minimum diameter for a carbon nanotube to get filled, thus making evident the more hydrophobic nature of such systems. Finally, we have also shown that the water molecules inside the tunnels are engaged in HB networks.

Financial support from ANPCyT (PME 2006-1581), MINCyT and CONICET is gratefully acknowledged. GAA, LMA and EPS are research fellows of CONICET.

## References

1. D.M. Huang, D. Chandler, Proc. Natl. Acad. Sci. U.S.A. **97**, 8324 (2000).
2. X. Huang, C.J. Margulis, B.J. Berne, Proc. Natl. Acad. Sci. U.S.A. **100**, 11953 (2003).
3. A. Bizzarri, S. Cannistraro, J. Phys. Chem. B **106**, 6617 (2002).
4. D. Vitkup, D. Ringe, G.A. Petsko, M. Karplus, Nat. Struct. Biol. **7**, 34 (2000).
5. N. Choudhury, B. Montgomery Pettitt, J. Phys. Chem. B **109**, 6422 (2005).
6. H.E. Stanley, P. Kumar, L. Xu, Z. Yan, M.G. Mazza, S.V. Buldyrev, S.-H. Chen, F. Mallamace, Physica A **386**, 729 (2007).
7. N. Giovambattista, P.G. Debenedetti, C.F. Lopez, P.J. Rossky, Proc. Natl. Acad. Sci. U.S.A. **105**, 2274 (2008).
8. J.C. Rasaiah, S. Garde, G. Hummer, Annu. Rev. Phys. Chem. **59**, 713 (2008).
9. J. Qvist, M. Davidovic, D. Hamelberg, B. Halle, Proc. Natl. Acad. Sci. U.S.A. **105**, 6296 (2008).
10. D.C. Malaspina, E.P. Schulz, L.M. Alarcón, M.A. Frechero, G.A. Appignanesi, Eur. Phys. J. E **032**, 35 (2010).
11. E. Schulz, M. Frechero, G. Appignanesi, Ariel Fernández, PLoS ONE **5**, e12844 (2010).
12. S. Vaitheeswaran, H. Yin, J.C. Rasaiah, G. Hummer, Proc. Natl. Acad. Sci. U.S.A. **101**, 17002 (2004).
13. G. Hummer, J.C. Rasaiah, J.P. Noworyta, Nature **414**, 188 (2001).
14. D. Takaiwa, I. Hatano, K. Koga, H. Tanaka, Proc. Natl. Acad. Sci. U.S.A. **105**, 39 (2008).
15. M. Rana, A. Chandra, J. Chem. Sci. **119**, 367 (2007).
16. A. Fernández, H.A. Scheraga, Proc. Nat. Acad. Sci. U.S.A. **100**, 113 (2003).
17. P. Ball, Nature **423**, 25 (2003).
18. W.L. Jorgensen, J. Chandrasekhar, J.D. Madura, R.W. Impey, M.L. Klein, J. Chem. Phys. **79**, 926 (1983).
19. M.W. Mahoney, W.L. Jorgensen, J. Chem. Phys. **112**, 8910 (2000).
20. H.J.C. Berendsen, J.P.M. Postma, W.F. van Gunsteren, A. DiNola, J.R. Haak, J. Chem. Phys. **81**, 3684 (1984).
21. D.A. Case, T.A. Darden, I.T.E. Cheatham, C.L. Simmerling, J. Wang, R.E. Duke, R. Luo, K.M. Merz, D.A. Pearlman, M. Crowley, R.C. Walker, W. Zhang, B. Wang, S. Hayik, A. Roitberg, G. Seabra, K.F. Wong, F. Paesani, X. Wu, S. Brozell, V. Tsui, H. Gohlke, L. Yang, C. Tan, J. Mongan, V. Hornak, G. Cui, P. Beroza, D.H. Mathew, C. Schafmeister, W.S. Ross, P.A. Kollman, AMBER9, University of California, San Francisco, CA (2006).